


Distinguishing the low-lying vector beauty-charm meson via polarization analysis

Yiqi Geng,¹ Mingqi Cao¹, and Ruilin Zhu^{1,2,3,*}

¹*Department of Physics and Institute of Theoretical Physics, Nanjing Normal University, Nanjing, Jiangsu 210023, China*

²*CAS Key Laboratory of Theoretical Physics, Institute of Theoretical Physics, Chinese Academy of Sciences, Beijing 100190, China*

³*Peng Huanwu Innovation Research Center, Institute of Theoretical Physics, Chinese Academy of Sciences, Beijing 100190, China*

 (Received 5 October 2023; accepted 1 April 2024; published 25 April 2024)

To distinguish the low-lying vector beauty-charm meson, we systematically study the $B_c^* \rightarrow B_c + \gamma$, $B_c^* \rightarrow \ell + \nu_\ell$, and $B_c^{(*)} \rightarrow J/\psi + nh$ processes within effective theory by the helicity decomposition method. The significant difference of polarization asymmetry in $B_c^{(*)} \rightarrow J/\psi + nh$ indicates a general law in vector-to-vector and pseudoscalar-to-vector transition processes, which can be tested in current and future LHC experiments. In the end, we discuss the experiment search and discovery potential for the low-lying vector beauty-charm meson.

DOI: [10.1103/PhysRevD.109.L071301](https://doi.org/10.1103/PhysRevD.109.L071301)

Introduction. Understanding of quantum chromodynamics (QCD) color confinement is one of the fundamental goals of particle physics. The low-lying vector beauty-charm meson B_c^* is believed to exist in various quark models and lattice simulations of first principles QCD but has not been identified in particle experiments. The B_c^* meson has become the last missing piece of the low-lying vector meson spectroscopy puzzle since the next to last vector ground state B_s^* was probed by the CUSB-II detector in 1990 [1].

The long-standing difficulties to discover the B_c^* meson come from two aspects. On the one hand, the B_c^* meson is produced in large quantities at hadron colliders while observation of the major decay channel $B_c^* \rightarrow B_c + \gamma$ is extremely difficult due to the low energy of the photon. The complete determination of both the emitted photon energy and the decay width is not given in literature. Recently, the second and third members of the beauty-charm meson family, i.e. first radially excited pseudoscalar and vector states $B_c(2S)$ and $B_c^*(2S)$, were just discovered and confirmed by investigating the $B_c + 2\pi$ invariant mass spectrum in CMS [2] and LHCb [3] experiments after previous pioneering observation of one excited peak at the ATLAS detector [4]. In both CMS and LHCb experiments,

two excited structures are observed but reconstruction of the $B_c^*(2S)$ state relies on the unknown photon due to $B_c^*(2S) \rightarrow B_c^*(\rightarrow B_c + \gamma) + 2\pi$, where the absolute mass satisfies $m_{B_c^*(2S)} = m_{B_c^*(2S)}|_{\text{rec}} + E_\gamma$ with the missing photon energy $E_\gamma = \Delta M_{b\bar{c}(1S)} = m_{B_c^*} - m_{B_c}$. Thus the probe of the B_c^* meson will affect the final determination of $B_c^*(2S)$ absolute mass. The precise study of hyperfine mass splitting is also helpful in understanding the low-energy effective theory of QCD.

On the other hand, the partial decay widths of weak decay channels such as $B_c^* \rightarrow J/\psi + X_{H,L}$ are expected to have same order of magnitude compared to that of the ground beauty-charm meson decays $B_c \rightarrow J/\psi + X_{H,L}$ with H (L) denoting hadrons (leptons). But the weak decay rates of B_c^* is suppressed by a factor $\Gamma(B_c)/\Gamma(B_c^*)$ with magnitude around 10^{-4} to 10^{-5} . Using the data sample corresponding to an integrated luminosity of 9 fb^{-1} , the LHCb Collaboration has successfully measured 36463 $B_c \rightarrow J/\psi + X_H$ weak decay events [5]. Thus one can expect several B_c^* weak decay events in LHCb Run-2 existing data samples. However, the reconstruction of B_c^* weak decay events is still challenging because the small hyperfine mass splitting of beauty-charm mesons leads to two relatively close peaks, and one peak is very high due to a large number of B_c decay events.

In this Letter, we present the important polarization analysis of B_c^* electromagnetic and weak decays. We generalize the low-energy effective theory for heavy quarkonium electromagnetic interactions into an unequal quark mass case. The decay width of radiative decay $B_c^* \rightarrow B_c + \gamma$ is investigated in a model-independent way, where the

*Corresponding author: rlzhu@njnu.edu.cn

Published by the American Physical Society under the terms of the [Creative Commons Attribution 4.0 International license](https://creativecommons.org/licenses/by/4.0/). Further distribution of this work must maintain attribution to the author(s) and the published article's title, journal citation, and DOI. Funded by SCOAP³.

dependence of B_c^* electromagnetic decay widths on the emitted photon energy is given. The weak decays of $B_c^{(*)} \rightarrow J/\psi + n\pi$ are studied in QCD effective theory. By fitting the $B_c \rightarrow J/\psi + 3\pi$ partial distribution data in the LHCb experiment, we can extract the spectra function of three pions. We find that the spectra function of three pions is major from two resonance contributions, i.e. the $a_1(1260)$ and $\pi_2(2005)$ states. By employing the helicity decomposition method, we find that the two kinds of channels $B_c^* \rightarrow J/\psi + n\pi$ and $B_c \rightarrow J/\psi + n\pi$ have extremely different polarization behavior dependence of the invariant mass of $n\pi$ system. The B_c^* meson can be distinguished in $J/\psi + n\pi$ invariant mass distributions by introducing a new polarization observable and measuring its value in particle experiments at the LHC.

Radiative decay. The lifetime of vector beauty-charm meson B_c^* is greatly shorter than that of the ground pseudoscalar beauty-charm meson B_c , since the B_c^* meson can first radiate into a B_c meson with several tens of MeV phase space while the B_c meson has to weak decay.

For the transition of doubly heavy quark mesons, potential nonrelativistic QCD (pNRQCD) is a powerful model-independent effective theory [6]. Its Lagrangian can be obtained by integrating out quarks and gluons of momentum and energy above heavy quark relative momentum from NRQCD [7], which is a nonrelativistic effective theory of QCD after integrating out quarks and gluons of momentum and energy above heavy quark mass. In pNRQCD effective theory, two fields $S = S(r, R, t)$ and $O = O(r, R, t)$ denoting the color singlet and octet quark-antiquark states respectively are introduced. r is the heavy quark relative coordinate while R is the center-of-mass coordinate. In the equal quark mass case, the pNRQCD Lagrangian relevant to describe the magnetic dipole transition at order $E_\gamma^3 v^2/m^2$ is systematically established in Ref. [8], where the radiative decay width is obtained as $\Gamma_{J/\psi \rightarrow \eta_c + \gamma} = (1.5 \pm 1.0)$ keV in excellent agreement with experimental data. We generalize the pNRQCD Lagrangian into the unequal quark mass case, and then the effective Lagrangian at order $E_\gamma^3 v^2/m^2$ can be written as

$$\begin{aligned} \mathcal{L}_{\gamma\text{pNRQCD}} = & \int d^3r \text{Tr} \left[e \frac{e_Q - e'_Q}{2} V_A^{\text{em}} S^\dagger \mathbf{r} \cdot \mathbf{E}^{\text{em}} S + e \left(\frac{e_Q m'_Q - e'_Q m_Q}{4m_Q m'_Q} \right) \left[V_S^{\frac{\sigma \cdot B}{m}} \{S^\dagger, \sigma \cdot \mathbf{B}^{\text{em}}\} S \right. \right. \\ & \left. \left. + \frac{1}{8} V_S^{(r \cdot \nabla)^2 \frac{\sigma \cdot B}{m}} \{S^\dagger, \mathbf{r}^i \mathbf{r}^j (\nabla^i \nabla^j \sigma \cdot \mathbf{B}^{\text{em}})\} S + V_O^{\frac{\sigma \cdot B}{m}} \{O^\dagger, \sigma \cdot \mathbf{B}^{\text{em}}\} O \right] \right. \\ & \left. + e \left(\frac{e_Q m_Q^2 - e'_Q m_Q^2}{32m_Q^2 m_Q'^2} \right) \left[4 \frac{V_S^{\frac{\sigma \cdot B}{m}}}{r} \{S^\dagger, \sigma \cdot \mathbf{B}^{\text{em}}\} S + 4 \frac{V_S^{\frac{\sigma \cdot (r \times r \times B)}{m^2}}}{r} \{S^\dagger, \sigma \cdot [\hat{\mathbf{r}} \times (\hat{\mathbf{r}} \times \mathbf{B}^{\text{em}})]\} S \right. \right. \\ & \left. \left. - V_S^{\frac{\sigma \cdot \nabla \times E}{m^2}} [S^\dagger, \sigma \cdot [-i \nabla \times, \mathbf{E}^{\text{em}}]] S - V_S^{\frac{\sigma \cdot \nabla_r \times r \cdot \nabla E}{m^2}} [S^\dagger, \sigma \cdot [-i \nabla_r \times, \mathbf{r}^i (\nabla^i \mathbf{E}^{\text{em}})]] S \right] \right. \\ & \left. + e \left(\frac{e_Q m_Q^3 - e'_Q m_Q^3}{8m_Q^3 m_Q'^3} \right) \left[V_S^{\frac{\nabla_r^2 \sigma \cdot B}{m^3}} \{S^\dagger, \sigma \cdot \mathbf{B}^{\text{em}}\} \nabla_r^2 S + V_S^{\frac{(\nabla_r \cdot \sigma)(\nabla_r \cdot B)}{m^3}} \{S^\dagger, \sigma^i \mathbf{B}^{\text{em}j}\} \nabla_r^i \nabla_r^j S \right], \end{aligned} \quad (1)$$

where Q and Q' denote two different heavy quarks.

The final result for the decay width of $B_c^*(p) \rightarrow B_c(p') + \gamma(k)$ is

$$\Gamma_{B_c^* \rightarrow B_c + \gamma} = \frac{\alpha(e_Q m'_Q - e'_Q m_Q)^2 E_\gamma^3}{3m_Q^2 m_Q'^2} V_S^{\frac{\sigma \cdot B}{m}} \left(1 - \frac{E_\gamma}{m_{B_c^*}} \right), \quad (2)$$

where the photon energy is expressed as $E_\gamma = \frac{m_{B_c^*}^2 - m_{B_c}^2}{2m_{B_c^*}}$. The

matching coefficient is known at one loop with $V_S^{\frac{\sigma \cdot B}{m}} = 1 + C_F \frac{\alpha_s}{2\pi}$ [9]. Other higher-order pNRQCD operators are not considered here; however, one can expect their contributions are small, similar to the case in bottomonium. We choose $Q = b$ and $Q' = c$ for beauty and charm quarks in the following.

The total decay width of the vector B_c^* meson can be approximated as $\Gamma \simeq \Gamma_{B_c^* \rightarrow B_c + \gamma}$ since other weak decay channels have a suppression factor $\Gamma(B_c)/\Gamma(B_c^*)$ with magnitude around 10^{-4} to 10^{-5} . Considering that the heavy quark pole mass is usually chosen as $m_b = 4.8 \pm 0.2$ GeV and $m_c = 1.6 \pm 0.1$ GeV, the total decay width of the vector B_c^* meson as a function of the emitted photon mass or hyperfine mass splitting is plotted in Fig. 1. If we choose the vector B_c^* meson mass as 6331(4) (6) MeV from lattice QCD simulation [10], the total decay width of the vector B_c^* meson is estimated as $\Gamma = 114_{-42}^{+60}$ eV where the large uncertainty is from the sensitivity of decay width on the meson mass. One should note that there are already several theoretical predictions [11–16]; however, the model-independent investigation is first given in our paper.

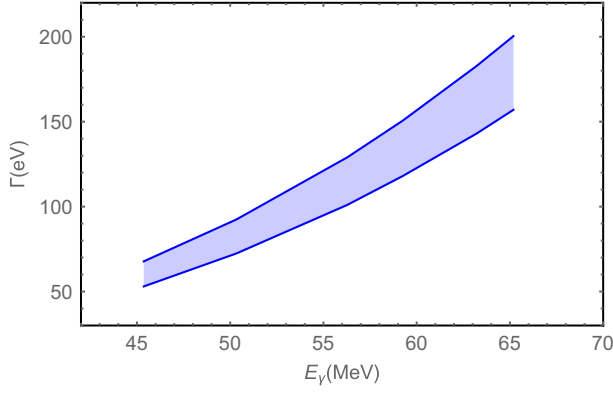


FIG. 1. Total decay width of the low-lying vector B_c^* meson as function of the emitted photon energy.

In calculation, only two polarization states of the vector B_c^* meson with $|J = 1, \lambda = \pm 1\rangle$ are equal contributions in the radiative B_c^* meson decays. In the rest frame of the final B_c meson, the angular momentum projection is identical to the vector B_c^* meson helicity λ . This phenomenon can be understood by the conservation of angular momentum and parity. Since the photon only has two transversal polarization statuses, the initial B_c^* meson with $|J = 1, \lambda = 0\rangle$ can not emit a photon parallel to the momentum direction and thus is forbidden in its radiative decay. The right-hand circularly polarized photon is emitted when the initial B_c^* meson with $|J = 1, \lambda = 1\rangle$ decays into a zero-spin B_c meson, while the left-hand circularly polarized photon is emitted when the initial B_c^* meson with $|J = 1, \lambda = -1\rangle$ decays into a zero-spin B_c meson.

Weak decay. In the radiative decay of the B_c^* meson with $B_c^* \rightarrow B_c + \gamma$, the transverse polarization of the B_c^* meson with $|J = 1, \lambda = \pm 1\rangle$ contributes, while the longitudinal polarization of the B_c^* meson with $|J = 1, \lambda = 0\rangle$ decouples. In the weak decays, both the transversely and longitudinally polarized B_c^* mesons will come in and contribute the Feynman amplitudes.

The pure leptonic weak decays $B_c^* \rightarrow \ell + \nu_\ell$ have been studied up to three-loop accuracy in Refs. [17,18], where the branching ratios are given with magnitude around 10^{-6} . If we focus on the polarization decomposition, the transverse and longitudinal polarizations of B_c^* meson leptonic decay widths are

$$\begin{aligned} \Gamma(B_c^*(\lambda = \pm 1) \rightarrow \ell \nu_\ell) &= \frac{|V_{cb}|^2}{12\pi} G_F^2 f_{B_c^*}^2 \left(1 - \frac{m_\ell^2}{m_{B_c^*}^2}\right)^2 m_{B_c^*}^3, \\ \Gamma(B_c^*(\lambda = 0) \rightarrow \ell \nu_\ell) &= \frac{m_\ell^2 \Gamma(B_c^{*+}(\lambda = \pm 1) \rightarrow \ell \nu_\ell)}{2m_{B_c^*}^2}, \end{aligned} \quad (3)$$

where the factor $(m_\ell/m_{B_c^*})^2$ in the longitudinal polarization formula represents a helicity suppression which is just a consequence of angular momentum conservation.

The weak decays into $B_c^* \rightarrow J/\psi + X_{H,L}$ are also good channels to probe the B_c^* meson at hadron colliders. The vector current form factors of B_c^* into J/ψ can be defined as

$$\begin{aligned} \langle J/\psi(\epsilon', p') | \bar{b} \gamma_\mu c | B_c^*(\epsilon, p) \rangle &= -(\epsilon \cdot \epsilon') [P_\mu V_1(q^2) - q_\mu V_2(q^2)] - (\epsilon \cdot q) \epsilon'^*_\mu V_3(q^2) \\ &+ (\epsilon'^* \cdot q) \epsilon_\mu V_4(q^2) + \frac{(\epsilon \cdot q)(\epsilon'^* \cdot q)}{M^2 - M'^2} \\ &\times \left[\left(P^\mu - \frac{M^2 - M'^2}{q^2} q^\mu \right) V_5(q^2) + \frac{M^2 - M'^2}{q^2} q^\mu V_6(q^2) \right], \end{aligned} \quad (4)$$

where $P = p + p'$, $q = p - p'$. M and M' are the masses of B_c^* and J/ψ respectively. Similarly, the axial-vector current form factors of B_c^* into J/ψ can be defined as

$$\begin{aligned} \langle J/\psi(\epsilon', p') | \bar{b} \gamma_\mu \gamma_5 c | B_c^*(\epsilon, p) \rangle &= i \epsilon_{\mu\nu\alpha\beta} \epsilon'^{\alpha} \epsilon'^{\beta} [P^\nu A_1(q^2) + q^\nu A_2(q^2)] \\ &+ \frac{i \epsilon_{\mu\nu\alpha\beta} P^\alpha q^\beta}{M^2 - M'^2} [\epsilon'^* \cdot q \epsilon^\nu A_3(q^2) - \epsilon \cdot q \epsilon'^*\nu A_4(q^2)]. \end{aligned} \quad (5)$$

The differential distribution for $B_c^{(*)} \rightarrow J/\psi + nh$ can be decomposed into

$$\frac{d\Gamma(B_c^{(*)} \rightarrow J/\psi + nh)}{dq^2} = \sum_{\lambda_i} \frac{|V_{cb}|^2 G_F^2 a_1^2 |\mathbf{p}'|}{32\pi M^2} \Gamma_{J_1 \lambda_1 J_2 \lambda_2 \lambda_{nh}}, \quad (6)$$

where the parameter $\Gamma_{J_1 \lambda_1 J_2 \lambda_2 \lambda_{nh}}$ is the helicity component with the initial meson angular momentum J_1 and the J/ψ angular momentum J_2 . The J/ψ moving momentum is $|\mathbf{p}'| = ((M^2 + M'^2 - q^2)^2 / (4M^2) - M'^2)^{1/2}$. Due to the angular momentum conservation, we have the following nontrivial helicity components:

$$\begin{aligned} \Gamma_{11110} &= 2[V_1^2((M - M')^2 - q^2)((M' + M)^2 - q^2) \\ &+ (A_1(M^2 - M'^2) + A_2 q^2)^2] \rho_T^{nh}(q^2), \end{aligned} \quad (7)$$

$$\begin{aligned} \Gamma_{1111t} &= 2[A_1^2(-2M^2(M'^2 + q^2) + (M'^2 - q^2)^2 + M^4) \\ &+ (V_1(M'^2 - M^2) + q^2 V_2)^2] \rho_L^{nh}(q^2). \end{aligned} \quad (8)$$

The other four nontrivial helicity components for vector B_c^* decay are complicated and are given in the Appendix. Here, $\lambda_{1,2} = 1$ represents $\lambda_{1,2} = \pm 1$. For pseudoscalar B_c decay, there are similar helicity components,

$$\Gamma_{00100} = \frac{\rho_T^{nh}(q^2)}{4M'^2(M'+M)^2} [-A_2'(M^4 - 2M^2(M'^2 + q^2) + (M'^2 - q^2)^2) + A_1'(M'+M)^2(M^2 - M'^2 - q^2)]^2, \quad (9)$$

$$\Gamma_{0010t} = \rho_L^{nh}(q^2)A_0'^2[-2M^2(M'^2 + q^2) + M^4 + (M'^2 - q^2)^2], \quad (10)$$

$$\Gamma_{00111} = \frac{2q^2\rho_T^{nh}(q^2)}{(M'+M)^2} [A_1'^2(M'+M)^4 + V'^2(M^4 - 2M^2(M'^2 + q^2) + (M'^2 - q^2)^2)], \quad (11)$$

where the definition of $B_c \rightarrow J/\psi$ form factors $A_i'(q^2)$ and $V'(q^2)$ can be found in Eqs. (2) and (3) in Ref. [19].

The above spectral functions $\rho_{T,L}^{nh}(q^2)$ are universal and can be defined as

$$\int \frac{d\Phi(W^* \rightarrow nh)}{2\pi} \epsilon_\mu^{nh} \epsilon_\nu^{*nh} = (q_\mu q_\nu - q^2 g_{\mu\nu}) \rho_T^{nh}(q^2) + q_\mu q_\nu \rho_L^{nh}(q^2). \quad (12)$$

In principle, the dimensionless spectral functions $\rho_{T,L}^{nh}(q^2)$ can be determined from nonperturbative calculation or experimental data. The LHCb Collaboration has studied the $B_c^+ \rightarrow J/\psi + \pi^+ + \pi^- + \pi^+$ process and measured the 3π invariant mass distribution in Ref. [20]. The polarization measurement of J/ψ is not performed in this process; however, the 3π distribution has a large peak around $a_1(1260)$ and a small peak around $\pi_2(2005)$ in Fig. 2. Thus we can conclude that the spectral function $\rho_T^{nh}(q^2)$ dominates in $B_c \rightarrow J/\psi + 3\pi$.

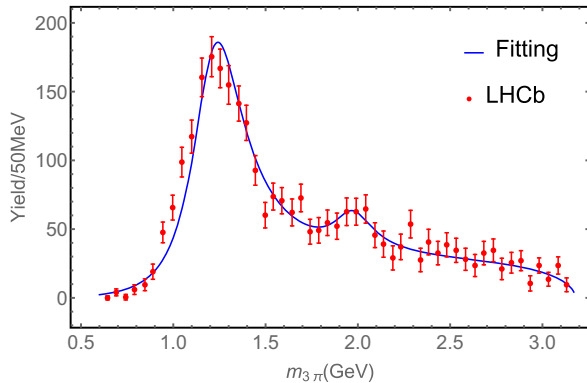


FIG. 2. The invariant mass distribution of $m_{3\pi}$ in the $B_c^+ \rightarrow J/\psi \pi^+ \pi^- \pi^+$ process. The red points are from the LHCb measurements based on the sample corresponding to an integrated luminosity of 9 fb^{-1} data [20], while the blue line is our fitting result.

We use the following parametrization form for $\rho_T^{3\pi}$:

$$\rho_T^{3\pi}(m^2) = \frac{a}{2m} \left(\frac{m^2 - m_\pi^2 e}{m^2} \right)^{-2} (1 - m^2 f) \times \left[\frac{1}{b^2/4 + (m - m_1)^2} + \frac{c}{d^2/4 + (m - m_2)^2} \right], \quad (13)$$

which is different to the form in Refs. [21,22]. If we input the two poles $m_1 = 1.209 \text{ GeV}$ and $m_2 = 1.963 \text{ GeV}$ for $a_1(1260)$ and $\pi_2(2005)$ peaks, the chi-square goodness of fitting is $\chi^2/\text{dof} = 1.65$. The parameters are fitted as $a = 0.12 \text{ GeV}$, $b = 0.341 \text{ GeV}$, $c = 0.021$, $d = 0.256 \text{ GeV}$, $e = -12.456$, and $f = -0.069 \text{ GeV}^{-2}$. Therein $b = 0.341 \text{ GeV}$ and $d = 0.256 \text{ GeV}$ can explain the decay width of $a_1(1260)$ and $\pi_2(2005)$ respectively. For future theoretical and experimental studies, this process can be employed to precisely measure the basic quantities for both the $a_1(1260)$ and $\pi_2(2005)$ states. Note that the value $a = 0.12 \text{ GeV}$ is obtained by considering the B_c hadroproduction cross section around 100 nb^{-1} at the LHC in Ref. [23].

Employing the $\rho(770)$ dominant model for $\rho_T^{2\pi}$,

$$\rho_T^{2\pi}(m^2) = \frac{a'}{\Gamma_\rho^2/4 + (m - m_\rho)^2}, \quad (14)$$

where the parameter $a' = 0.1198 \text{ GeV}^2$ can be extracted from the theoretical prediction of $B_c \rightarrow J/\psi + \rho$ in Ref. [24].

The nontrivial results of various form factors at leading order can be calculated in NRQCD,

$$\begin{aligned} V_1(y) &= \frac{128\pi(z+1)^{5/2} \alpha_s \phi_{1_{S_0[c\bar{c}]}}^{(0)}(0) \phi_{1_{S_0[c\bar{b}]}}^{(0)}(0)}{3z^{3/2} m_b^3 (y-z+1)^2 (y+z-1)^2}, \\ V_3(y) &= 2V_1(y) = 2A_1(y), \\ V_2(y) &= A_2(y) = \frac{1-z}{1+z} V_1(y), \\ V_4(y) &= \frac{4z}{1+z} V_1(y), \end{aligned} \quad (15)$$

where $z = m_c/m_b$ and $y = \sqrt{q^2/m_b^2}$. The HPQCD Collaboration has performed the first lattice calculation of $B_c \rightarrow J/\psi$ form factors [25]. In previous works [19,24,26–28], various $B_c \rightarrow J/\psi$ form factors have been systematically studied by the NRQCD + HPQCD approach along with the Boyd-Grinstein-Lebed parametrization method [29]. Similarly, we can further determine the $B_c^* \rightarrow J/\psi$ form factors after combining the lattice QCD results of $B_c \rightarrow J/\psi$ form factors and NRQCD relations among form factors. High-order calculation affects the NRQCD relations among form factors vary slightly.

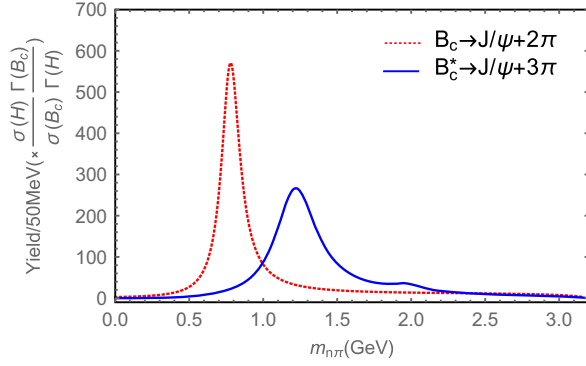


FIG. 3. The reconstruction events distribution for both the $B_c \rightarrow J/\psi + 2\pi$ and $B_c^* \rightarrow J/\psi + 3\pi$ at LHCb run-2.

According to the LHCb reconstruction efficiency in Ref. [20], the event yields per every 50 MeV can also be obtained for both the $B_c \rightarrow J/\psi + 2\pi$ and $B_c^* \rightarrow J/\psi + 3\pi$ processes, which have been plotted in Fig. 3.

The helicity formula for the decay width is given in Eq. (6). One can further define the polarization asymmetry α_{LT} as

$$\alpha_{LT} = \frac{\sum_{\lambda_1, \lambda_{nh}} \Gamma_{J_1 \lambda_1 11 \lambda_{nh}} - \Gamma_{J_1 \lambda_1 10 \lambda_{nh}}}{\sum_{\lambda_1, \lambda_{nh}} \Gamma_{J_1 \lambda_1 11 \lambda_{nh}} + \Gamma_{J_1 \lambda_1 10 \lambda_{nh}}}, \quad (16)$$

where we only observe the transverse and longitudinal polarization of J/ψ due to its feasibility at particle experiments.

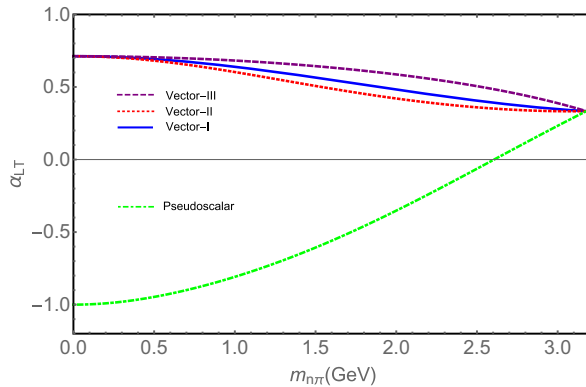


FIG. 4. The polarization asymmetry α_{LT} is significantly different in the two processes $B_c^* \rightarrow J/\psi + n\pi$ and $B_c \rightarrow J/\psi + n\pi$ with $n = 2$ or $n = 3$. In $B_c \rightarrow J/\psi + n\pi$ decays, the polarization asymmetry α_{LT} denoting ‘‘Pseudoscalar’’ are not sensitive to the relative magnitude between the $n\pi$ spectra functions $\rho_{L,T}(q^2)$. While in $B_c^* \rightarrow J/\psi + n\pi$ decays, the polarization asymmetry α_{LT} is slightly sensitive to the spectra functions, where ‘‘Vector-I, Vector-II, Vector-III’’ represent $\rho_L = \rho_T$, $\rho_L = \rho_T/10$, $\rho_L = 10\rho_T$, respectively.

We plot the results of α_{LT} of $B_c^* \rightarrow J/\psi + n\pi$ and $B_c \rightarrow J/\psi + n\pi$ with $n = 2$ or $n = 3$ in Fig. 4. In calculation, we found that J/ψ prefers to be longitudinally polarized in B_c decays while J/ψ prefers to be transversely polarized in B_c^* decays, which indicates a general law of polarization asymmetry for pseudoscalar (vector) meson to vector meson decays. In $P \rightarrow V$ transition, the final vector meson V prefers longitudinal polarized and goes to 100% longitudinal polarized ($\alpha_{LT} = -1$) in a maximum recoil point ($q^2 = 0$). In $V \rightarrow V'$ transition, the final vector meson V' prefers transversely polarized and gets a large polarized rate ($0.5 < \alpha_{LT} < 1$) in a maximum recoil point ($q^2 = 0$). This general law shall be also tested in various processes such as $B_s/B_s^* \rightarrow D_s^* + nh$, $B/B^* \rightarrow D^* + nh$, $D_s/D_s^* \rightarrow \phi + nh$, and $D/D^* \rightarrow K^* + nh$.

Going back to the identification of the B_c^* meson, one may expect around 20 $B_c^* \rightarrow J/\psi + \pi$ and 280 $B_c^* \rightarrow J/\psi + \ell + \nu_\ell$ at LHCb run-2, assuming 9×10^8 B_c^* mesons are produced [23]. However, only 1 $B_c^* \rightarrow J/\psi + \pi$ and 11 $B_c^* \rightarrow J/\psi + \ell + \nu_\ell$ can be reconstructed if one considers the LHCb efficiency in Ref. [5]. The reconstruction events will increased into 33 times in future LHCb run-3 and run-4 experiments. The polarization measurement of J/ψ will eliminate the possible B_c background to probe the B_c^* meson. Apart from the channels in the paper, one can also probe the B_c^* meson by $B_c^* \rightarrow B_s/B + n\pi$ with around 10^{-5} branching ratios.

Conclusion. In this paper the electromagnetic and weak decays of B_c^* are studied in a model-independent way. We have shown the helicity decomposition in $B_c^* \rightarrow B_c + \gamma$, $B_c^* \rightarrow \ell + \nu_\ell$, and $B_c^* \rightarrow J/\psi + nh$ by polarization analysis. The polarization asymmetry α_{LT} introduced in the paper is an important physical observable for distinguishing the initial pseudoscalar B_c and vector B_c^* states. It also reveals a general law in $P \rightarrow V$ and $V \rightarrow V'$ transition processes, which can be tested by the polarization measurements of the final vector mesons. In the end, the long-sought vector B_c^* meson has a good opportunity to be resolved during LHCb run-3 or run-4 and future experiments such as CEPC running at a Z boson pole.

Acknowledgments. We thank Prof. Chao-Hsi Chang and Prof. Bing-Song Zou for valuable discussions. This work is supported by NSFC under Grant No. 12322503, No. 12047503, and No. 12075124, and by Natural Science Foundation of Jiangsu under Grant No. BK20211267.

Appendix: The other four helicity components in Eq. (6) have the following expressions:

$$\begin{aligned}
\Gamma_{10111} &= \frac{q^2 \rho_T^{nh}(q^2)}{2M^2(M^2 - M'^2)^2} [2A_1(M^2 - M'^2)(3M^2 + M'^2 - q^2)((A_2 - 2A_4)M^2 q^2 + (A_2 + A_4)(M^2 - M'^2)^2 \\
&\quad - (A_2 + 2A_4)q^2 M'^2 + A_4 q^4) + ((A_2 - 2A_4)M^2 q^2 + (A_2 + A_4)(M^2 - M'^2)^2 - (A_2 + 2A_4)q^2 M'^2 + A_4 q^4)^2 \\
&\quad + A_1^2(M^2 - M'^2)^2(3M^2 + M'^2 - q^2)^2 + V_3^2(M - M')^2(M' + M)^2((M - M')^2 - q^2)((M' + M)^2 - q^2)], \\
\Gamma_{10100} &= \frac{(-2M^2(M'^2 + q^2) + M^4 + (M'^2 - q^2)^2)\rho_T^{nh}(q^2)}{16M^2 M'^2 (M^2 - M'^2)^2} [(M - M')(M' + M)(M^2(2V_1 - V_3 + V_4) \\
&\quad + (2V_1 + V_3 - V_4)M'^2 + q^2(-2V_1 + V_3 + V_4)) + V_5((M - M')^2 - q^2)((M' + M)^2 - q^2)]^2, \\
\Gamma_{1010r} &= \frac{\rho_L^{nh}(q^2)}{16M^2 M'^2} [2M^2((-V_3 + V_4 + V_6)M'^2 + q^2(V_1 + V_2 - V_3 + V_4 + V_6)) + M^4(-2V_1 - V_3 + V_4 + V_6) \\
&\quad + (M'^2 - q^2)((2V_1 + V_3 - V_4 - V_6)M'^2 + q^2(2V_2 - V_3 + V_4 + V_6))]^2, \\
\Gamma_{11101} &= \frac{q^2 \rho_T^{nh}(q^2)}{2M^2(M^2 - M'^2)^2} [2A_1(M^2 - M'^2)(M^2 + 3M'^2 - q^2)(-q^2(2A_3(M^2 + M'^2) + A_2(M^2 - M'^2)) + A_3 q^4 \\
&\quad + (A_2 + A_3)(M^2 - M'^2)^2) + (A_3 q^4 - q^2(2A_3(M^2 + M'^2) + A_2(M^2 - M'^2)) + (A_2 + A_3)(M^2 - M'^2)^2)^2 \\
&\quad + A_1^2(M^2 - M'^2)^2(M^2 + 3M'^2 - q^2)^2 + V_4^2(M^2 - M'^2)^2((M - M')^2 - q^2)((M' + M)^2 - q^2)].
\end{aligned}$$

-
- [1] J. Lee-Franzini, U. Heintz, D. M. J. Lovelock, M. Narain, R. D. Schamberger, J. Willins, C. Yanagisawa, P. Franzini, and P. M. Tuts, *Phys. Rev. Lett.* **65**, 2947 (1990).
- [2] A. M. Sirunyan *et al.* (CMS Collaboration), *Phys. Rev. Lett.* **122**, 132001 (2019).
- [3] R. Aaij *et al.* (LHCb Collaboration), *Phys. Rev. Lett.* **122**, 232001 (2019).
- [4] G. Aad *et al.* (ATLAS Collaboration), *Phys. Rev. Lett.* **113**, 212004 (2014).
- [5] R. Aaij *et al.* (LHCb Collaboration), *J. High Energy Phys.* **07** (2020) 123.
- [6] N. Brambilla, A. Pineda, J. Soto, and A. Vairo, *Nucl. Phys.* **B566**, 275 (2000).
- [7] G. T. Bodwin, E. Braaten, and G. P. Lepage, *Phys. Rev. D* **51**, 1125 (1995); **55**, 5853(E) (1997).
- [8] N. Brambilla, Y. Jia, and A. Vairo, *Phys. Rev. D* **73**, 054005 (2006).
- [9] A. V. Manohar, *Phys. Rev. D* **56**, 230 (1997).
- [10] N. Mathur, M. Padmanath, and S. Mondal, *Phys. Rev. Lett.* **121**, 202002 (2018).
- [11] D. Ebert, R. N. Faustov, and V. O. Galkin, *Phys. Rev. D* **67**, 014027 (2003).
- [12] L. P. Fulcher, *Phys. Rev. D* **60**, 074006 (1999).
- [13] S. S. Gershtein, V. V. Kiselev, A. K. Likhoded, and A. V. Tkabladze, *Phys. Usp.* **38**, 1 (1995).
- [14] S. Godfrey, *Phys. Rev. D* **70**, 054017 (2004).
- [15] E. J. Eichten and C. Quigg, *Phys. Rev. D* **49**, 5845 (1994).
- [16] Z. G. Wang, *Eur. Phys. J. C* **73**, 2559 (2013).
- [17] W. Tao, R. Zhu, and Z. J. Xiao, *Phys. Rev. D* **106**, 114037 (2022).
- [18] W. Tao, Z. J. Xiao, and R. Zhu, *J. High Energy Phys.* **05** (2023) 189.
- [19] W. Wang and R. Zhu, *Int. J. Mod. Phys. A* **34**, 1950195 (2019).
- [20] R. Aaij *et al.* (LHCb Collaboration), *J. High Energy Phys.* **01** (2022) 065.
- [21] A. V. Luchinsky, *Phys. Rev. D* **86**, 074024 (2012).
- [22] A. V. Luchinsky, *Phys. Lett. B* **832**, 137269 (2022).
- [23] C. H. Chang and X. G. Wu, *Eur. Phys. J. C* **38**, 267 (2004).
- [24] C. F. Qiao, P. Sun, D. Yang, and R. L. Zhu, *Phys. Rev. D* **89**, 034008 (2014).
- [25] J. Harrison *et al.* (HPQCD Collaboration), *Phys. Rev. D* **102**, 094518 (2020).
- [26] D. Shen, H. Ren, F. Wu, and R. Zhu, *Int. J. Mod. Phys. A* **36**, 2150135 (2021).
- [27] R. Y. Tang, Z. R. Huang, C. D. Lü, and R. Zhu, *J. Phys. G* **49**, 115003 (2022).
- [28] C. F. Qiao and R. L. Zhu, *Phys. Rev. D* **87**, 014009 (2013).
- [29] C. G. Boyd, B. Grinstein, and R. F. Lebed, *Phys. Rev. D* **56**, 6895 (1997).